Numerical simulation of a thermoviscoelastic frictional problem with application to the hot-embossing process for manufacturing of microcomponents

Kabanemi, Kalonji; Marcotte, Jean-Philippe; Hétu, Jean-Francois; Worgull, M.; Heckele, M.

Publisher's version / Version de l'éditeur:
http://dx.doi.org/10.3139/217.2227
International Polymer Processing, 2009, 2, pp. 174-184, 2009

K. K. Kabanemi[*1], *J. P. Marcotte*[1], *J. F. Hétu*[1], *M. Worgull*[2], *M. Heckele*[2]

[1] *Industrial Materials Institute, National Research Council of Canada, Boucherville, Canada*
[2] *Institut fur Mikrostruktur-Technik, Karlsruhe, Germany*

Numerical Simulation of a Thermoviscoelastic Frictional Problem with Application to the Hot-Embossing Process for Manufacturing of Microcomponents

Hot embossing is a compression molding technique used for high replication accuracy of small features. One of the most sensitive phases of the process is the de-embossing stage during which the patterned part has to be demolded. In this paper, the demolding stage is considered as a frictional contact problem between a rigid mold insert and a viscoelastic polymer sheet as it deforms and cools inside a mold under an applied force. The contact is modeled with a modified Coulomb's law of dry friction while a generalized Maxwell model is used to describe the polymer behavior during embossing, cooling and de-embossing stages. The heat transfer between the mold insert and the patterned polymer sheet is solved through a domain decomposition method. A finite element approximation based on a penalized technique is proposed and analyzed. The purpose of this modeling approach is to predict dimensional stability and residual shape of microcomponents in the hot embossing process. Such a prediction will allow one to assign appropriate processing conditions that minimize geometrical imperfections and increase replication accuracy.

1 Introduction

The hot embossing process has been studied extensively over the last few years due to excellent replication accuracy and because of high aspect ratios that can be achieved for the manufacturing of microcomponents, compared with injection molding. Hot embossing process is essentially the stamping under a high pressure of a pattern into a polymer sheet that is held just above its glass transition temperature, T_g. Throughout the process, the polymer sheet undergoes simultaneous mechanical, rheological and thermal changes. After cooling the polymer below T_g, the pressure is released and the patterned polymer sheet is removed from the mold insert. The stamp (mold insert) used to define the pattern in the polymer may be made in variety of ways including laser micromachining, mechanical micromachining and lithographic methods. A schematic view of the process is shown in Fig. 1. We shall not describe the process any further. A thorough description may be found elsewhere (Heckele and Schomburg, 2004; Heckele et al., 1998; Schift et al., 2001; Studer et al., 2002; Scheer and Schulz, 2001; Juang et al., 2002a; Juang et al., 2002b).

In the hot embossing process, the replication accuracy depends on the ability to efficiently combine the sequence of embossing temperature, embossing pressure and embossing time, in order to prevent the occurrence of defects such as poor replication, geometrical imperfections, warpage and excessive molded-in stresses. We have been interested in understanding the role of frictional contact between the mold insert and the patterned polymer sheet during de-embossing since it significantly affects the replication accuracy and surface quality of microstructures. In this regard, numerical modeling can give useful insight in the overall process and help defining optimal design parameters that improve the replication accuracy. In the present study, we wish to benefit from progress made in numerical modeling of materials processing, to develop new numerical tools designed particularly for embossed components with micro-scale size feature, with an emphasis on the de-embossing stage. The objective is to relate final properties of the replication to the design parameters, i. e., the processing conditions, the polymer rheology and the interaction between contacting surfaces. Therefore, for the sake of clarity, we will find it useful to develop the basic equations for the model problem shown in Fig. 1B, along with different numerical techniques used.

In this study, a numerical approach for predicting deformations induced in a patterned polymer sheet during the replication of microstructures by hot embossing is presented. Only the compression phase, when the polymer sheet has already filled the small features of the mold insert is examined (Fig. 1B), along with the de-embossing process. Therefore, the paper is concerned with a frictional contact problem be-

* Mail address: Kalonji K. Kabanemi, Industrial Materials Institute, National Research Council of Canada, 75, de Martagne, Boucherville, Québec, Canada J4B 6Y4
E-mail: kalonji.kabanemi@nrc.ca

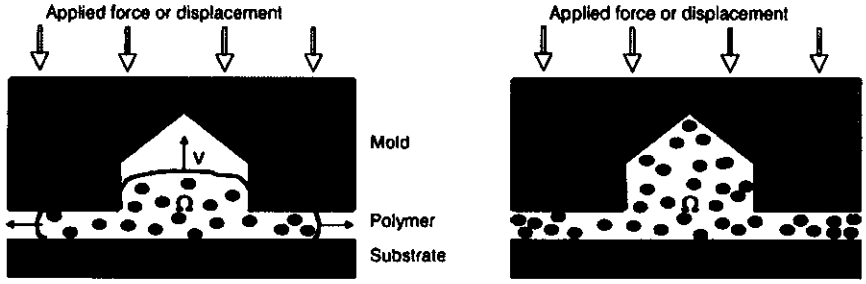

Fig. 1. Schematic view of the hot embossing problem

tween a rigid mold insert and a viscoelastic polymer sheet as it deforms and cools inside a mold under an applied force or pressure. The model takes into account phenomena associated with non-isothermal stress relaxation (Kovacs, 1958; Kabanemi and Crochet, 1992; Isayev, 1987; Ferry, 1970; Struik, 1990). Rheological characterization of the polymeric material is carried out in the range of the embossing temperatures, i.e., the glass transition temperature, to get useful insight of the material behavior during the process. In addition, a model is proposed to predict the frictional forces between the mold insert and the patterned polymer sheet as it deforms and cools inside the mold insert up to the moment of de-embossing. Though penalty procedures may induce problems associated with penalty sensitivity and possible ill conditioning of the matrix that is obtained from the finite element discretization of the problem, they were successfully used to enforce the contact condition.

In addition to numerical investigations, embossing experiments have been carried out to establish the relationship between various combinations of processing conditions and the fidelity of pattern transfer. The experiments were carried out with two different machines, i.e., an Instron machine and a commercial hot embossing machine, i.e., EVG-520 (Jaloux-Salard, 2005). As an illustration, a qualitative comparison between the numerical prediction and experimental data for an embossed microstructure is presented along with other relevant output emphasizing the effects of the three major design parameters, i.e., the embossing temperature, embossing pressure and the friction properties of contacting surfaces, on the replication accuracy.

2 Basic Equations

2.1 Integral Constitutive Model

In order to describe the behavior of a viscoelastic polymer sheet as it deforms and cools inside a mold insert under an applied force or pressure, an expression for the stress tensor has to be specified. We recall that, only the deformation phase, when the polymer sheet has already filled the small features of the mold insert is concerned, along with the de-embossing stage. The setting is as follows. A viscoelastic body occupies the full domain cavity, Ω (i.e. the cavity is completely filled as shown in Fig. 1B), and is acted upon by given forces, tractions and thermal solicitations (Fig. 1B). We assume that a quasi-static process is valid. We further assume that during the hot embossing process the polymer behaves as an isotropic thermorheologically simple material, in such a manner that stress components are related to histories of strain components and temperature through appropriate relaxation functions. The latter are derived from isothermal relaxation functions by assuming time-temperature equivalence on the basis of the WLF equation (Kovacs, 1958; Kabanemi and Crochet, 1992; Isayev, 1987; Ferry, 1970; Struik, 1990). On that basis, one obtains the general form of the constitutive equations for thermorheologically simple materials. Let us denote by s and s_{ij} the spherical and the deviatoric components of the stress tensor, σ, respectively, while e and e_{ij} denote the spherical and the deviatoric components of the strain tensor, ε, respectively. For an isotropic material, we use relaxation functions G_1 and G_2 in shear and dilatation respectively, together with a modified time-scale, ξ. Following Kabanemi and Crochet (1992), the stress–strain relation is expressed as

$$s_{ij}(x,t) = \int_{-\infty}^{t} G_1(\xi - \xi') \frac{\partial e_{ij}(x,t')}{\partial t'} dt', \tag{1}$$

$$s(x,t) = \int_{-\infty}^{t} G_2(\xi - \xi') \frac{\partial}{\partial t'} [e(x,t') - e_{th}(x,t')]\, dt'. \tag{2}$$

In Eq. 2, $e_{th} = \alpha\, \Delta T$, is the thermal strain tensor which depends upon the entire temperature history of the material point and not on the temperature T at time t alone (α being the thermal expansion coefficient) and ξ is the modified time scale at a given position, x, and is defined by

$$\xi(x,t) = \int_{0}^{t} \Phi[T(x,\lambda)]\, d\lambda. \tag{3}$$

In Eq. 3, T is the temperature field and Φ the shift function often characterized by the WLF equation written as follows

$$\log \Phi = \frac{c_1 (T - T_r)}{(c_2 + T - T_r)}. \tag{4}$$

where c_1 and c_2 are material constants and T_r is a reference temperature, that can be different from the glass transition temperature, T_g.

We wish to briefly comment on the relaxation functions G_1 and G_2 in Eqs. 1 and 2. Let 2μ and 3κ denote the value of G_1 and G_2 at time $t = 0$, respectively. In order to simplify the system of equations, we assume that

$$G_1(t) = \frac{E}{1+\nu} \varphi(t) = 2\mu\varphi(t), \tag{5}$$

$$G_2(t) = \frac{E}{1-2\nu} \varphi(t) = 3\kappa\varphi(t), \tag{6}$$

where both G_1 and G_2 depend upon the same relaxation function $\varphi(t)$. In Eqs. 5 and 6, E and ν are Young's modulus and Poisson's ratio, respectively, and μ and κ are shear and bulk modulus, respectively. We further decompose below the function $\varphi(t)$ as a sum of m exponentials, i.e.

$$\varphi(t) = \sum_{r=1}^{m} g_r \exp(-t/\theta_r), \tag{7}$$

in which θ_r are relaxation times and g_r material constants. We define partial stress components s_{ij}^r and sr associated with each relaxation time θ_r as

$$s_{ij} = \sum_{r=1}^{m} g_r s_{ij}^r, \tag{8}$$

$$s = \sum_{r=1}^{m} g_r s^r, \tag{9}$$

where

$$s_{ij}^r(x,t) = \int_{-\infty}^{t} 2\mu \exp\{-[\xi(x,t) - \xi(x,t')]/\theta_r\} \frac{\partial e_{ij}(x,t')}{\partial t'} dt', \tag{10}$$

$$s^r(x,t) = \int_{-\infty}^{t} 3\kappa \exp\{-[\xi(x,t) - \xi(x,t')]/\theta_r\} \times \frac{\partial}{\partial t'}[e(x,t') - e_{th}(x,t')]\, dt'. \tag{11}$$

2.2 *Contact and Fiction Formulation*

In the present formulation of the hot-embossing process, it is assumed that the mold insert and the substrate behave as rigid bodies (Fig. 1). We consider the case of a unilateral contact, which involves no penetration between the two bodies and is modeled with the Signorini conditions (Amassad and Fabre, 2003). We start our analysis by considering that a full contact zone, Γ, is developed at the entire interface between the polymer sheet and the mold insert. The first condition to satisfy is the non-penetration condition. Let n the interior normal to the mold insert that depends on the node under consideration. That normal can easily be obtained once the mold insert geometry is defined. Under these hypotheses, the non-penetration boundary conditions on Γ can be written as

$$u_n \leq 0, \tag{12}$$

$$f_n \leq 0, \tag{13}$$

$$f_n \cdot u_n = 0. \tag{14}$$

Here u_n is the normal displacement at the interface and f_n is the normal contact force. The first inequality, Eq. 12, represents the kinematic condition of no penetration of the contact surface. The second inequality, Eq. 13, is the static condition of compressive or zero normal tractions. The third equation, Eq. 14, states that there is zero work done by the normal contact stress, i.e., the normal contact stresses exist only at the nodes where the polymer sheet is in contact with the rigid mold insert.

We model the frictional contact between the viscoelastic body and the mold insert with a Coulomb's law of dry friction, written as

$$|f_t| < \mu_s |f_n|. \tag{15}$$

Here μ_s is a static friction coefficient associated with the stick friction constraint and f_t represents the tangential force on the contact boundary Γ. This static version of the Coulomb's law states that the tangential shear cannot exceed the maximal frictional resistance. When the strict inequality, $|f_t| < \mu_s|f_n|$, holds the surface adheres to the mold insert and is in the so-called stick state, and when the inequality, $|f_t| \geq \mu_s|f_n|$, holds there is relative sliding, the so-called slip state. The Coulomb's friction law is modified to include a dynamic friction coefficient μ_d associated with the slip condition when the static constraint is violated. In that case the inequality, $\mu_d \leq \mu_s$, holds. It follows from the above analysis that the interface mold/polymer is divided in three zones, which are not known *a priori* and are part of the problem: stick, slip and no contact or gap.

We use the penalty method to enforce contact constraints and a regularization technique to obtain estimates for the normal contact force, f_n, and the tangential frictional traction, f_t, as follows

$$f_n = -\lambda_n u_n, \tag{16}$$

$$f_t = -\lambda_t u_t, \tag{17}$$

where $\lambda_n > 0$ and $\lambda_t > 0$ are normal and tangential penalty parameters, respectively. The result is a solution to the contact problem that allows small violations of the contact constraints in order to estimate the direction and magnitude of the actual tractions. The physical significance of the tangential penalty parameter λ_t is that it represents the distributed tangential stiffness of the microstructure contact interface with the mold insert and therefore serves a double role of penalty parameter and microstructure stiffness parameter in the contact-friction algorithm. If the penalty is chosen too small there is unacceptable overlap, if it is chosen too large, one gets convergence problems.

2.3 *Conservation Equations*

The mechanical problem of frictional contact of the viscoelastic body may be formulated as follows. Find a displacement vector $\mathbf{u}$, and a stress field σ such that

$$\nabla \cdot \sigma + \mathbf{f} = 0 \quad \text{in } \Omega, \tag{18}$$

with the following boundary conditions:

$$u_n \leq 0, \quad f_n \leq 0, \quad f_n \cdot u_n = 0, \quad \text{on } \Gamma,$$

$$\text{if} \quad |f_t| \leq \mu_s |f_n| \Rightarrow u_t = 0,$$

$$\text{if} \quad |f_t| \geq \mu_s |f_n| \Rightarrow \exists \lambda_t > 0, \quad \text{such that } f_t = -\lambda_t u_t.$$

The equilibrium equation, Eq. 18, is solved along with the following energy equation

$$\rho c \frac{\partial T}{\partial t} = \nabla \cdot (k \nabla T), \tag{19}$$

where ρ, c and k are the density, the heat capacity and the thermal diffusivity respectively and the symbol ∇ is the gradient operator.

We wish to briefly comment on Eq. 19. The deformation (shrinkage and warpage) that occurs during solidification of the patterned polymer sheet in the mold insert causes a gap between the two bodies. A sharp temperature drop may occur across the gap depending on its thickness, as a result of the thermal contact resistance. Although the gap is known as the 'air gap', in many instances, there is probably no air in it. In our numerical simulation, the thermal conductivity of the gap medium is taken as that of air. It is clear that the gap at the mold/part interface will reduce the cooling rate and increase the cooling time of the part. The gap computed at the interface mold/part can be used in the heat transfer calculations. The heat flux across the interface is expressed as

$$q = -k\frac{\partial T}{\partial n} = \frac{k}{\Delta}(T_P - T_m) = h(T_P - T_m), \tag{20}$$

where Δ is the gap thickness, k is the thermal conductivity, h is the heat transfer coefficient and T_P and T_m are polymer and mold insert temperature, respectively. In our numerical simulations the heat transfer coefficient has been set to a constant value.

3 Solution Procedure for the Contact Problem

When the polymer sheet becomes in contact with the mold insert, a contact zone develops around the first contact point. An automatic procedure has been developed in order to track the nonlinear boundary conditions at the interface. We adopt here the procedure developed by Brunet (1992) and Kloosterman (2002). In that procedure, the decision on whether a contact node is releasing or is in sticking or sliding condition is based on the following decision tree:

- If $f_n \geq 0$ the point is assumed to have experienced tension release and in this case the penalty parameters and the normal and tangential contact force are set to zero.
- If $f_n \leq 0$ and $|f_t| \leq \mu_s|f_n|$ the node continues to stick and Eqs. (16 and 17 give appropriate estimations to the normal force and frictional traction. Sticking contact conditions must be assumed by setting the penalty parameters to a large positive number.
- If $f_n \leq 0$ and $|f_t| \geq \mu_s|f_n|$ then the state of the node must be updated to sliding with the consistent tangential penalty parameter $\lambda_t = \mu_d|f_n|/|u_t|$.

4 Space and Time Discretizations

The system of equations, Eqs. 18 and 19, is solved with a decoupled approach using a time-dependent algorithm. The energy equation is first solved using an implicit Euler scheme for the time integration and standard Galerkin finite element formulation for the space discretization. The heat transfer between mold and part is obtained through a domain decomposition method (Smith et al., 1996; Quarteroni and Valli, 1999). That is, the energy equation is solved iteratively on mold and part domains, exchanging interface temperature at each iteration, until convergence is achieved. The equilibrium equations are then integrated with a known temperature field using the standard Galerkin method.

Before we get to that point, we have to integrate the stress constitutive equations consisting of Eqs. 10 and 11. Their discretization in time between instants $t = t_n$ and $t = t_{n-1}$, leads to

$$\sigma_{ij}^{r,n} = L_{ij}^{r,n-1} + 2\mu Y_2^{r,n}\Delta\varepsilon_{ij}^n + \left(-\frac{2}{3}\mu + \kappa\right) Y_2^{r,n}\Delta\varepsilon_{mm}^n\delta_{ij} - \kappa Y_2^{r,n}\Delta e_{th}^n\delta_{ij}, \tag{21}$$

where the passed memory of deformations $L_{ij}^{r,n-1}$ is given by

$$L_{ij}^{r,n-1} = Y_1^{r,n}s_{ij}^{r,n-1} + \frac{1}{3}Y_1^{r,n}s^{r,n-1}\delta_{ij}. \tag{22}$$

The discrete relaxation functions $Y_1^{r,n}$ and $Y_2^{r,n}$ in Eqs. 21 and 22 are given by

$$Y_1^{r,n} = Y_2^{r,n} = \frac{1}{1 + \Delta\xi_n/\theta_r}. \tag{23}$$

This leads to a stable scheme for all modified time steps $\Delta\xi_n$.

A more accurate time-integration method (second order) for the constitutive equations, which gives a stable solution leads to (Kabanemi and Crochet, 1992)

$$Y_1^{r,n} = \exp(-\Delta\xi_n/\theta_r), \tag{24}$$

$$Y_2^{r,n} = [1 - \exp(-\Delta\xi_n/\theta_r)]\frac{\theta_r}{\Delta\xi_n}. \tag{25}$$

We recall that, during cooling and de-embossing the contact area is not known *a priori*, nor are the friction forces or the contact state (contact, no-contact, sliding, sticking). The contact algorithm given in previous section has been implemented with an incremental displacements approach in the finite element code. The algorithm is fully based on standard finite elements and requires only modifications of the contributions to the force vector and the stiffness matrix, respectively, associated with the contact nodes. A regularization technique as described in the previous section is employed to take into account the condition $f_t = -\mu_d|f_n|\frac{u_t}{|u_t|}$ in finite element calculations.

5 Hot Embossing Experiments

In this part, embossing experiments are carried out to establish the relationship between various combinations of processing conditions and fidelity of pattern transfer. Two different machines, i.e., a modified Instron machine and a commercial hot embossing machine (EVG-520) are used to carry out the embossing experiments. A thorough description of experimental devices is given by Jaloux-Salard (2005). The polymer used is a PMMA (Acrylite M-30), for which the glass transition temperature, of about 95 °C, was characterized using differential scanning calorimetry (DSC). The mold insert used to define the pattern in the polymer sheet was made by mechanical machining. Its surface was not very smooth as shown in Fig. 2. The surface roughness was then used to measure the replication accuracy, by scanning electron micrograph technique (SEM) photos of the embossed microcomponents. The main dimensions of a single square pin of the mold insert were 1×1 mm and 1 mm of height (Fig. 2).

Fig. 2. Scanning electron micrograph (SEM) picture of the square grid pattern mold insert

Fig. 3. SEM pictures of embossed PMMA microstructures showing a portion of the grid pattern at embossing temperature of 115 °C and embossing pressure of 20 kN

5.1 Hot Embossing with EVG-520 Machine

Using the commercial hot embossing machine, the fabricated microstructures showed excellent surface quality under embossing temperature of 115 °C, embossing pressure of 20 kN and holding time of 20 min, as shown in Fig. 3. The other combination of processing conditions gave only poor replication accuracy as can be seen in Figs. 4 and 5. More precisely, for embossing temperature around T_g, for which the material has a higher modulus, visible cracks were observed on the surface of microstructures (see Fig. 5). Increasing the embossing temperature above 115 °C resulted in a much better replication while increasing the cycle time. Because of the high level of residual stresses induced in the microstructures in such conditions, the de-embossing process itself was no longer easy.

5.2 Hot Embossing with Instron Machine

The embossing experiments with the modified Instron machine produced excellent surface quality under embossing temperature of 100 °C, embossing pressure of 2.4 kN and 7 min of holding time, as shown in Fig. 6. As can be seen from this replication picture, less severe processing conditions for temperature, pressure and holding time with our modified Instron machine, produced high replication quality compared to the replication with the commercial EVG machine. The noticeable difference between experimental results from these two devices, at same processing conditions, highlighted in Figs. 4B and 6, is due essentially to temperature control of the patterned polymer sheet (by means of a thermoelectric cooler) and embossing time during which the pressure was maintained constant to compensate for the material shrinkage due to cooling inside the mold insert. It follows from these two series of experiments that to better produce high replication accuracy of microstructures, the sequence of embossing temperature, embossing pressure and embossing time have to be controlled carefully. This control needs an accurate determination of the contact zone along with the friction effects between contacting surfaces. This issue is addressed in the following section devoted to numerical simulation.

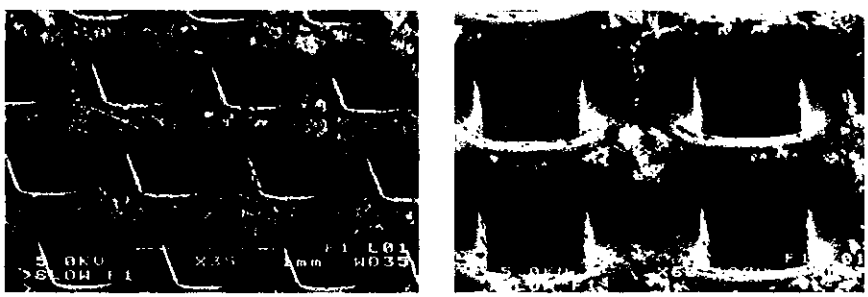

A) B)

Fig. 4. SEM pictures of embossed PMMA microstructures showing a portion of the grid pattern at embossing pressure of 2.5 kN and embossing temperature of: (A) 95 °C, and (B) 100 °C

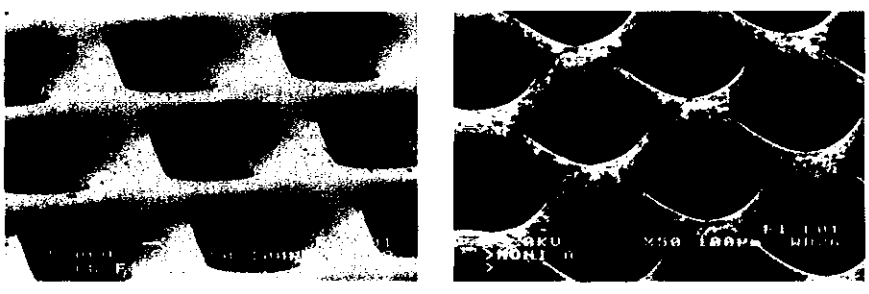

A) B)

Fig. 5. SEM pictures of embossed PMMA microstructures showing a portion of a grid pattern at embossing temperature of 95 °C and embossing pressure of: (A) 20 kN, and (B) 30 kN

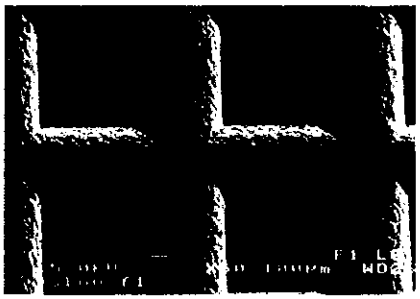

Fig. 6. SEM pictures of embossed PMMA microstructures showing a portion of a grid pattern at embossing temperature of 100 °C, embossing pressure of 2.4 kN and holding time of 5 min

6 Numerical Results and Discussion

Several embossing problems, with and without frictional contact, were solved numerically to demonstrate the effectiveness of the numerical approach discussed above and to study the effects of different processing conditions on the replication accuracy. The polymer used in this study is a PMMA, whose physical data are given in the Appendix. We have adopted a relaxation spectrum characterized by four relaxation times.

6.1 Square Hole Grid Pattern

As first application, we study the cooling of a 3 × 3 square hole grid pattern inside a mold insert along with the de-embossing stage, with an emphasis on the frictional contact between the microstructure and the mold insert. This application is an idealized problem of our previous experimental microstructure. The objective is to show the efficiency of the method developed for solving thermoviscoelastic small strain frictional contact problem. In what follows, the effects of processing conditions on the overall replication quality are investigated. The geometry and boundary conditions of the frictional contact problem are depicted in Fig. 7. The main dimensions of a single square hole of the microstructure were 1 × 1 mm and 1 mm of depth. We start the analysis by considering that a full contact zone is present at the entire interface between the microstructure shown in Fig. 7A and the mold insert (not shown). We recall that the lateral outer surfaces of the microcomponent are considered as free during the entire process (see Fig. 7A for details). For the sake of simplicity in creating the mesh depicted in Fig. 7A, no demolding angle has been designed contrary to the mold insert photograph in Fig. 2. Accordingly, high stresses are expected during embossing and de-embossing stages.

6.2 Free Cooling Inside the Mold Insert without an Applied Force

At first, we only study a free cooling inside the mold insert of the microcomponent depicted in Fig. 7A without an applied force, followed by the de-embossing stage. The microcomponent is initially at temperature 183 °C, while the reference temperature is set to 90 °C. The total cooling time inside the mold,

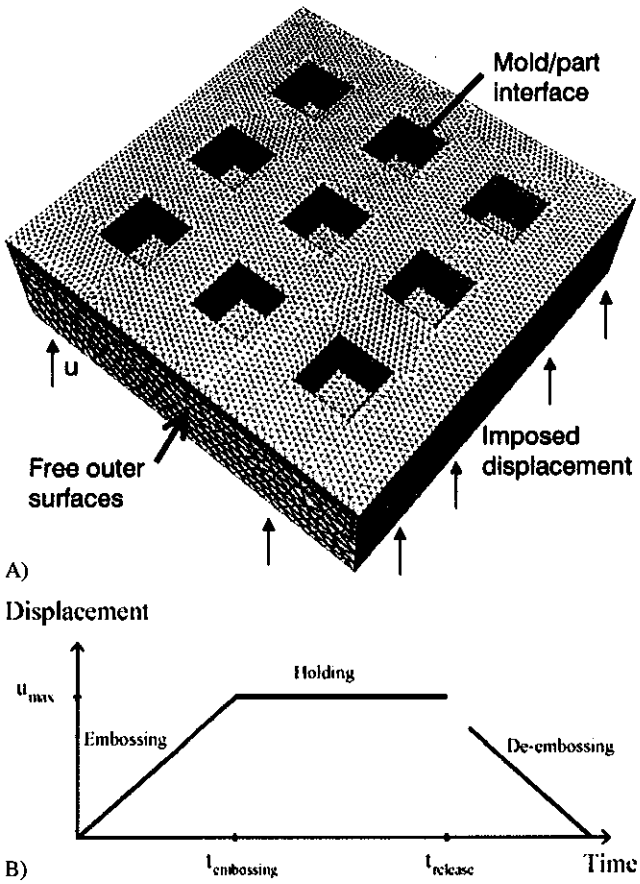

Fig. 7. Geometry of the square hole grid pattern and finite element mesh (A). The main dimensions of a single square hole of the microstructure were 1 × 1 mm and 1 mm of depth, and (B) Graphic of processing conditions used for cooling of microcomponents under an applied force

without an applied force, is 20 s. The duration of de-embossing stage depends on how long it takes for the part to be removed from the mold insert. Unless otherwise stated, the penalty parameter for normal and frictional contact is set to 1000, and the static and dynamic friction coefficients are 0.3 and 0.1, respectively. Numerical results are summarized in Figs. 8 to 10. The deformed configurations of the microstructure and the gap formation at two stages during cooling inside the mold are shown in Fig. 8 (only a half of the cross section is shown). We have superimposed in the same figure the original shape (in wire frame) and the deformed shape of the microcomponent, to emphasize the gap formation at the contacting surfaces during cooling. Since we are analyzing free cooling of the microcomponent, a gap is developed at the bottom of contacting surfaces and along the lateral contacting surfaces as a result of shrinkage of microstructures, while a fully contacting surface still persists in the upper region of the mold insert (re-entrant corners) and the microstructures. The prediction of contact and no contact regions is of great interest, as it affects the surface quality during sliding of the two bodies in the de-embossing stage. The stress distribution at the end of cooling inside the mold insert (t = 20 s) and after 5 s during de-embossing is shown in Fig. 9. In this figure, complex deformations of outer microstructures are apparent. Tensile stresses are developed

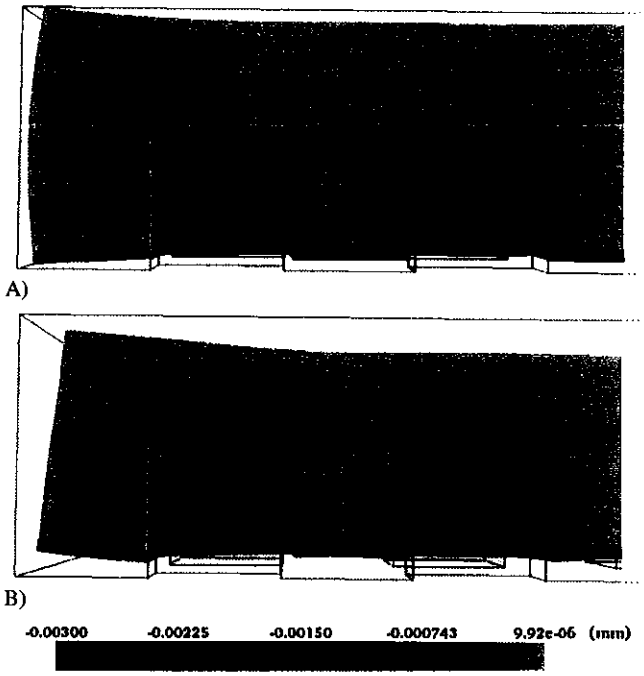

Fig. 8. Half cross section of the microstructure showing the gap formation at the interface between the mold insert and the microcomponent during cooling at two different times: (A) t = 5 s and (B) t = 20 s (end of cooling inside the mold). The deformation has been amplified by a factor of 20 (initial shape of the microcomponent in wire frame)

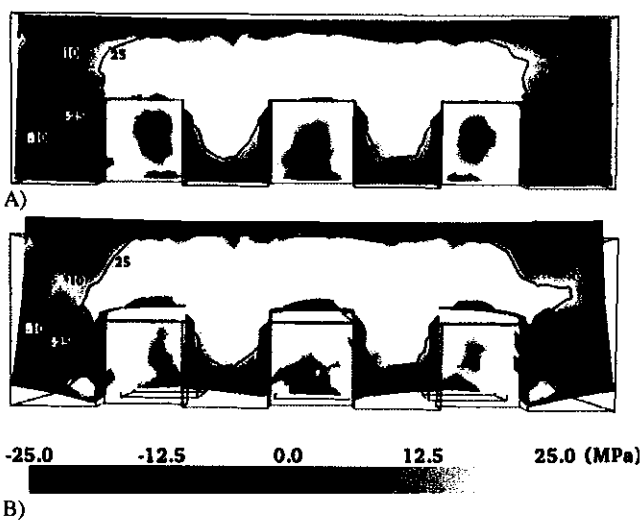

Fig. 9. Cross section of the microcomponent showing the stress field: (A) end of cooling inside the mold insert (t = 20 s), and (B) after 5 s during de-embossing stage. The deformation has been amplified by a factor of 5 (initial shape of the microcomponent in wire frame)

around the corners of the microstructures as a consequence of the mold core, which prevents free deformations of the part. The effect of friction between the mold insert and the microstructure at a given time during de-embossing is shown in Fig. 10. Results with and without friction are very different. More precisely, the re-entrant corners of microstructures, which exhibit large frictional force, experience large deformations. In particular, the outer microstructures are more de-

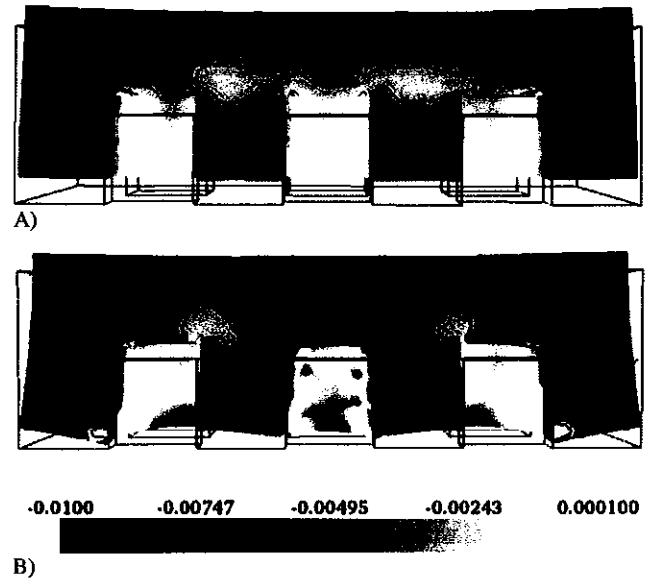

Fig. 10. Cross section of the microstructure showing the effect of frictional force on the deformation of the microcomponent at a given time during de-embossing: (A) without friction ($\mu_s = 0$ and $\mu_d = 0$), and (B) with friction ($\mu_s = 0.3$ and $\mu_d = 0.1$). The deformation has been amplified by a factor of 5 (initial shape of the microcomponent in wire frame)

formed than the inner ones (Fig. 10B). When de-embossing is performed without friction coefficient, all microstructures experience almost the same deformation as shown in Fig. 10A.

6.3 Role of the Embossing Force

A second series of numerical simulation concern the cooling of the microcomponent under an applied force. Since we are mainly interested in the coupling effects of pressure, temperature and friction on the replication quality, we shall now study the role of the embossing pressure alone. A vertical displacement is therefore applied at the top of microstructure during the cooling inside the mold, followed by the de-embossing stage. The graphic of the processing condition is shown in Fig. 7B. The other conditions are as before. In Fig. 11A we show the distribution of the stress field at the end of embossing (t = 20 s). As stated before, since no demolding angle is present in the microstructures, very large stresses are predicted accordingly. The combined effect of embossing force and frictional contact on the deformation of the outer microstructures is emphasized in that figure. In particular, noticeable differences are obtained for the overall deformation of the microcomponent compared to deformation in free cooling inside the mold (see Fig. 9A), which exhibited a smaller deformation of outer microstructures. The deformed configurations of the microcomponent at different stages during de-embossing are shown in Figs. 11B and C. We basically observe three zones. The first corresponds to the gap (no contact zone). In this zone, the normal and tangential forces are zero. The second and third correspond to the contacting zone. In these zones, nodes continue to stick or to slide depending on whether or not the Coulomb friction law is verified. Large stresses are predicted around edges

due to the mold insert core that prevents the part from deforming freely. There is no tangential displacement at this node until the tangential frictional force reaches the value $\mu_s|f_n|$, and then sliding occurs. During sliding, we observe a re-distribution and a partial relaxation of stresses in the part. At the beginning of de-embossing, the contact between the mold insert and the part is only localized near corner and higher friction forces are developed in these regions. Therefore, it can be expected that the replication in these regions will not be of good quality as can be seen in Fig. 11C. Therefore, the geometrical imperfection can be predicted by means of the amplitude of the friction force at the interface of contacting surfaces. The effect of embossing force at a given contacting node is depicted in Fig. 12. As we vary the embossing force, we only get a small effect on the frictional contact force and on the overall deformation.

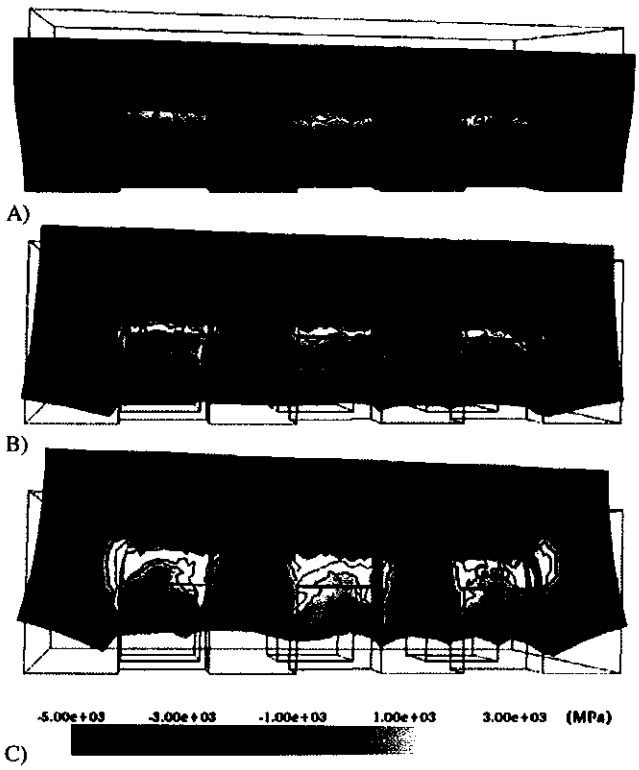

Fig. 11. Cross section of the microstructure showing the deformation of the microcomponent at three different stages during embossing and the distribution of the stress field: (A) end of cooling inside mold (t = 20 s), (B) after 10 s during de-embossing and (C) after 20 s during de-embossing. The deformation has been amplified by a factor of 3 (initial shape of the microcomponent in wire frame)

6.4 Role of the Embossing Temperature and Friction Coefficient

As we stated earlier, the replication quality is very sensitive to embossing temperature and friction at contacting surfaces. The effects of embossing temperature and friction coefficient are depicted in Figs. 13 and 14. The evolution of the frictional contact forces at three different embossing temperatures is shown in Fig. 13. It appears from that figure that, the frictional

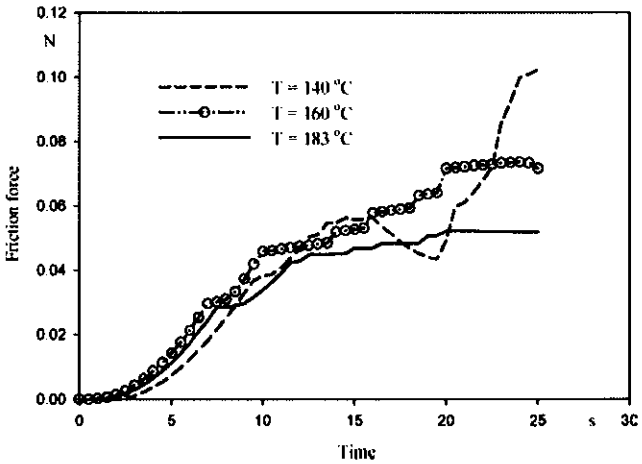

Fig. 13. Evolution of the friction force at a contacting node during cooling (t ≤ 20 s) and de-embossing (t > 20 s). Effect of the embossing temperature

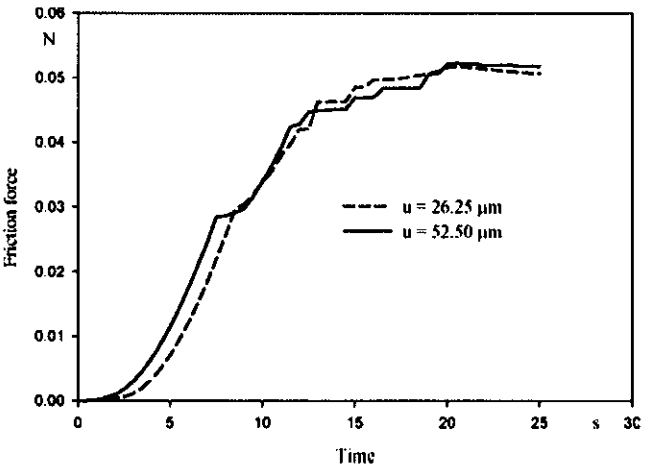

Fig. 12. Evolution of the friction force at a contacting node during cooling (t ≤ 20 s) and de-embossing (t > 20 s). Effect of the embossing force

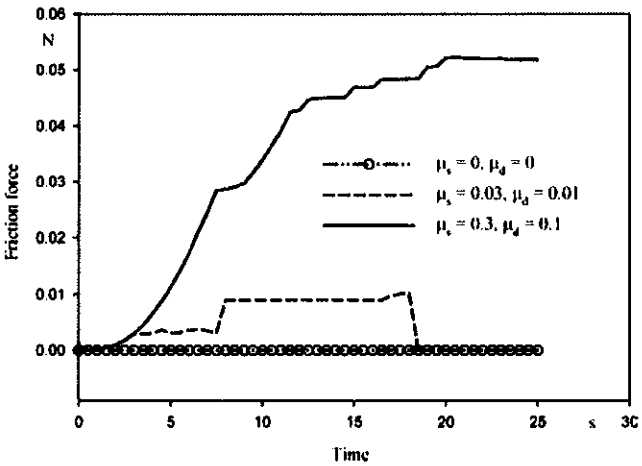

Fig. 14. Evolution of the friction force at a contacting node during cooling (t ≤ 20 s) and de-embossing (t > 20 s). Effect of the coefficient of friction between contacting surfaces

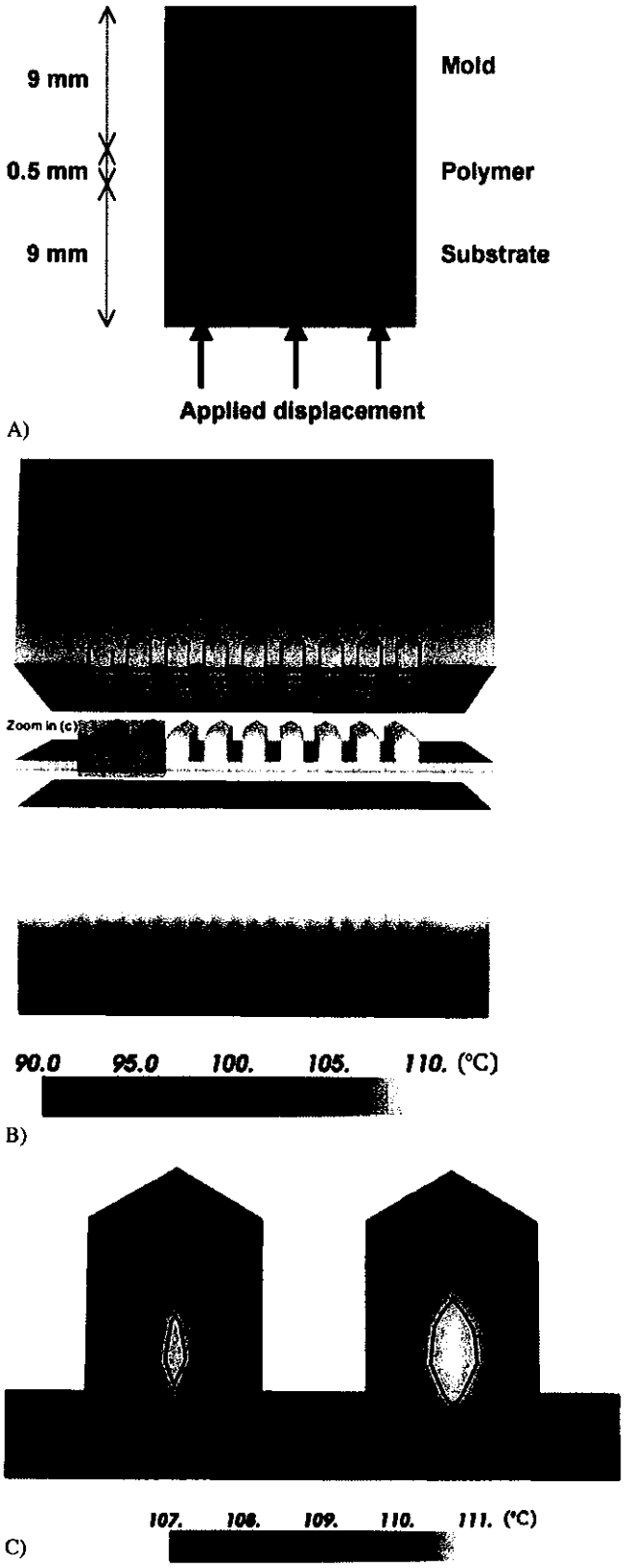

Fig. 15. Problem definition (A), cross section of the mold insert (B) and microstructures with temperature distribution at t = 20 s during cooling, and (C) zoomed view of the temperature distribution in the cross section of the two microstructures highlighted in B)

forces increase monotonically as the part cools down inside the mold under an applied force. During de-embossing (t > 20 s), for an embossing temperature of 140 °C (close to T_g), the frictional force increases very rapidly. Such a frictional force may induce cracks and large deformations on the surface of microstructures, resulting in poor replication. A similar behavior was reported in our experiments, where we examined the role of the embossing temperature on the fidelity of the replication (see Fig. 5). In Figs. 10 and 14, we analyze the effect of the friction coefficient on the frictional contact force developed at the mold/part interface. The same conclusions can be drawn for the frictional force at contacting surfaces, which shows similar qualitative trends to what we reported for the effect of embossing temperature. As a result, the embossing temperature and the friction coefficient between the master and the replica are the major parameters that strongly influence the embossing process. The numerical experiments suggest reducing the interfacial forces between the master and the replica in order to ensure a clean de-embossing process and to reduce the residual stresses, which have negative effect on the replication quality.

6.5 Micro-pin Pattern

We examine in this sub-section the replication of micro-pin structures, whose geometry and dimensions are shown in Fig. 15A. The initial residual layer before we apply the normal force is 500 μm. First, a displacement is applied stepwise at the bottom side of the contact body until the holding force reaches a prescribed value (embossing time is set to 20 s). Then, the holding pressure is kept constant during 20 s while cooling the microstructure (see Fig. 7B). The other conditions and material properties are as before. The temperature field after 20 s during cooling is shown in Figs. 15B and C, which emphasize the heat transfer between the mold insert and the microstructures. The shear stress field after 40 s during cooling inside the mold is shown in Fig. 16. These results correspond to the viscoelastic calculation without friction. As can be seen from this figure, microstructures in the central region behave almost in the same way, while those localized near boundaries exhibit high shear stresses. We also observe that residual stresses are localized around bottom corners in all microstructures. The effect of friction on residual stresses and deformations is analyzed in Fig. 17. In particular, all microstructures behave almost in the same way when friction is taken into account. Fig. 18 shows a

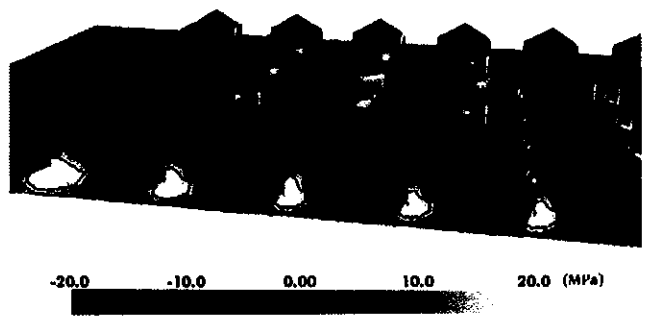

Fig. 16. Shear stresses in a cross section at t = 40 s, during cooling under an applied force, without friction ($\mu_s = 0$ and $\mu_d = 0$)

cross section of the deformed geometry at various steps during de-embossing stage along with the gap formation at the interface of the microstructures and the mold. We have superimposed in the same figure the original shape (in wire frame) and the deformed shape of the microstructures, to emphasize the gap formation at the contacting surfaces. It is apparent that microstructures are subjected to a very complex deformation history. The same conclusions to what we reported in the previous simulation can be drawn for the frictional contacting areas, which exhibit similar qualitative trends, i.e., a sticking region on re-entrant corners in which $|f_t| \leq \mu_s|f_n|$, a sliding region in the bottom area in which $|f_t| \geq \mu_s|f_n|$ and a loss of contact area (gap) in the central region. Inspection of Fig. 18 shows that the contact force exerted by the mold insert on the microstructure is mainly localized around the bottom re-entrant corners. While a nearly perfect contact is observed for outer microstructures, inner microstructures exhibit larger gap in the upper region with an average of about 1.5 μm (Fig. 18A). As the de-embossing stage progresses, the microstructures get more and more deformed (Figs. 18B and C), with outer microstructures exhibiting larger deformations.

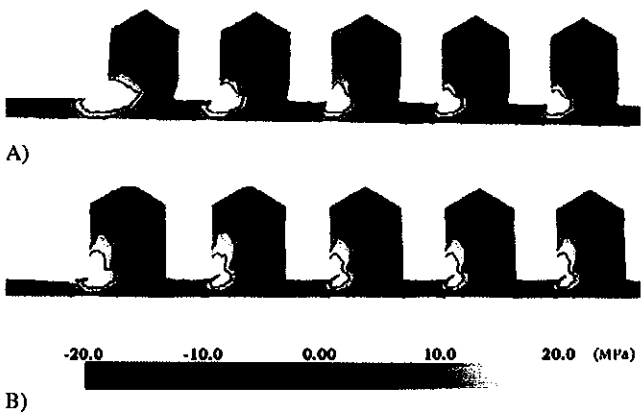

Fig. 17. Shear stresses in a cross section at t = 40 s, during cooling under an applied force: (A) without friction ($\mu_s = 0$ and $\mu_d = 0$) and (B) with friction ($\mu_s = 0.3$ and $\mu_d = 0.1$)

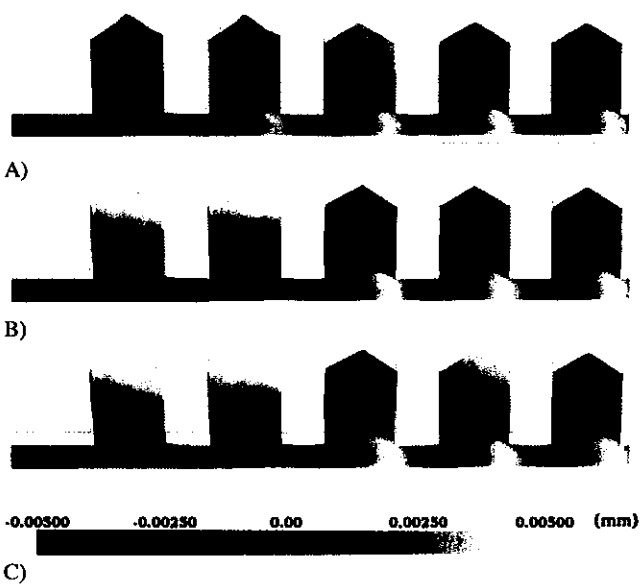

Fig. 18. Half cross section of the microcomponent showing the deformation of microstructures at different stages during de-embossing and the distribution of horizontal displacement field: (A) t = 50 s, (B) t = 55 s and (C) t = 60 s. The deformation has been amplified by a factor of 3 (initial shape of the microcomponent in wire frame)

7 Conclusion

In this paper a solution of a viscoelastic frictional problem with application to the hot embossing process has been proposed. Numerical results, obtained with an experimental microstructure geometry, have shown the effectiveness of the method. Frictional forces between the mold insert and the substrate strongly influence the overall deformations during cooling inside the mold insert. Our results have also shown that residual stresses are mainly localized around corners of microstructures and that, outer microstructures exhibit higher shear stresses and larger deformations. The numerical procedure developed provides a tool for studying the importance of processing conditions and of the nature contact surface on the replication quality, i.e., deformation, frictional forces and residual stresses. More precisely, the replication quality is more sensitive to the variation of the embossing temperature and the friction between the master and the replica, followed by the embossing force.

Appendix

The material data used in the present paper correspond to a PMMA (Kabanemi et al., 2005). They are collected bellow. On the basis of an experimental master curve for PMMA at 110 °C, obtained by Kabanemi et al. (2005), we have adopted a relaxation function characterized by four relaxation times. Referring to Eq. 7, we have:

$\theta_1 = 1.66 \cdot 10^6$ s, $g_1 = 4.22 \cdot 10^{-3}$,

$\theta_2 = 1.97 \cdot 10^{-1}$ s, $g_2 = 8.20 \cdot 10^{-1}$,

$\theta_3 = 1.10 \cdot 10^1$ s, $g^3 = 1.62 \cdot 10^{-1}$,

$\theta_4 = 2.59 \cdot 10^3$ s, $g_3 = 1.36 \cdot 10^{-2}$.

Material data	Symbol	Value
Young's modulus	E	$1.9732 \cdot 10^9$ Nm^{-2}
Poisson's ratio	ν	0.38
Density (average value)	ρ	$1.18 \cdot 10^3$ kg m^{-3}
Specific heat (average value)	c	2500 J kg^{-1} K^{-1}
Thermal conductivity (average value)	k	0.16 W m^{-1} K^{-1}
Glass transition temperature	T_g	113 °C
Thermal expansion coefficient	α	$7 \cdot 10^{-5}$ °C^{-1}
WLF coefficient	c_1	12.79
WLF coefficient	c_2	74.78 °C

Table A1. Material data for the PMMA

References

Amassad, A., Fabre, C., "Analysis of a Viscoelastic Unilateral Contact Problem Involving the Coulomb Friction Law", J. Opt. Theor. Appl., **116**, 465–483 (2003)

Brunet, M., "Numerical Analysis of Cold-Forming Residual Stresses in Thin-Walled Structures", in Numiform'92 Proceedings, Chenot (Eds.), Balkema, Rotterdam, p. 427–432 (1992)

Ferry, J. D.: Mechanical Properties of Polymers, 2nd Edition, Willy & Sons (1970)

Heckele, M., Schomburg, W. K., "Review on Micro Molding of Thermoplastic Polymers", J. Micromech. Microeng., **14**, R1–R14 (2004)

Heckele, M., et al., "Hot Embossing – The Molding Technique for Plastic Microstructures", Microsyst. Technol., **4**, 122–124 (1998).

Isayev, A. I.: Injection and Compression Molding Fundamentals. Marcel Dekker, New York (1987)

Jaloux-Salard, M. A.: Étude Expérimentale et Théorique du Procédé de Matriçage à Chaud de Thermoplastiques pour la Fabrication de Microstructures. Bachelor Thesis, École d'ingénieurs en génie des systèmes industriels, La Rochelle, France (2005)

Juang, Y. J., et al., "Hot Embossing in Microfabrication. Part I: Experimental", Polym. Eng. Sci., **42**, 539–550 (2002a)

Juang, Y. J., et al., "Hot Embossing in Microfabrication. Part II: Rheological Characterization and Process Analysis", Polym. Eng. Sci., **42**, 539–550 (2002b)

Kabanemi, K. K., Crochet, M. J., "Thermoviscoelastic Calculation of Residua Stresses and Residual Shapes of Injection Molded Parts", Int. Polym. Proc., **7**, 60–70 (1992)

Kabanemi, K. K., et al., "Numerical Simulation of a Thermoviscoelastic Frictional Problem with Application to the Hot-Embossing Process for Microstructure Fabrication", Americas Regional Meeting PPS Proceedings (2005)

Kloosterman, G.: Contact Methods in Finite Element Simulations. Ph.D. Thesis, Netherlands Institute for Metals Research (2002)

Kovacs, A. J., "La Contraction Isotherme du Volume des Polymères Amorphes", J. Polym. Sci., **30**, 131–147 (1958)

Quarteroni, A., Valli, A.: Domain Decomposition Methods for Partial Differential Equations. Clarendon Press, Oxford (1999)

Scheer, H.-C., Schulz, H., "A Contribution to the Flow Behaviour of thin polymer films during hot embossing lithography", Microelectron. Eng., **56**, 311–332 (2001)

Schift, H., et al., "Pattern Formation in Hot Embossing of Thin Polymer Films", Nanotechnology, **12**, 173–177 (2001)

Smith, B., et al.: Domain Decomposition, Parallel Multilevel Methods for Elliptic Partial Differential Equations. Cambridge University Press (1996)

Struik, L. C. E.: Internal Stresses, Dimensional Instabilities and Molecular Orientations in Plastics. Willy & Sons (1990)

Studer, V., et al., "Nanoembossing of Thermoplastic Polymers for Microfluidic Applications", Appl. Phys. Lett., **80**, 3614–3616 (2002)

Date received: September 10, 2008
Date accepted: January 6, 2009

Bibliography
DOI 10.3139/217.2227
Intern. Polymer Processing
XXIV (2009) 2; page 174–184

ISSN 0930-777X